Scientific paper

# A New Multifunctional Phenanthroline-Derived Probe for Colorimetric Sensing of Fe<sup>2+</sup> and Fluorometric Sensing of Zn<sup>2+</sup>

Chen-Yu Qi,<sup>†,1</sup> Xue Dong,<sup>†,1</sup> Ying-Cui Fan,<sup>1</sup> Jun-Ru Yuan,<sup>1</sup> Zi-Jie Song,<sup>1</sup> Yong-Han Zhang,<sup>1</sup> Ya-Ping Xie,<sup>1</sup> Feng Yang,<sup>1</sup> Jian-Ping Ma,<sup>2,\*</sup> Meng Wang<sup>1,\*</sup> and Jie Qin<sup>1,\*</sup>

<sup>1</sup> School of Life Sciences and Medicine, Shandong University of Technology, Zibo 255049, P. R. China

<sup>2</sup> College of Chemistry, Chemical Engineering and Materials Science, Key Laboratory of Molecular and Nano Probes, Shandong Normal University, Jinan 250014, P. R. China

\* Corresponding author: E-mail: ddress: xxgk123@163.com; wm902012@163.com; qinjiesdut@163.com Tel.: 0086-533-2786607; Fax: 0086-533-2781329.

† These authors contributed equally to this work.

Received: 02-22-2024

#### **Abstract**

A new phenanthroline derivative bearing imidazole group, (2-(3,5-di(pyridin-4-yl)phenyl)-1-p-tolyl-1H-imidazo[4,5-f] [1,10]phenanthroline) has been devised. The derivative serves as a multifunctional probe, exhibiting a highly sensitive colorimetric response to Fe<sup>2+</sup> ion and a selectively ratiometric fluorescent response to Zn<sup>2+</sup> ion in a buffer-ethanol solution. The colorless-to-red visual color change upon addition of Fe<sup>2+</sup> accompanied by enhanced absorption makes this derivative a suitable naked-eye sensor for Fe<sup>2+</sup> ion. Moreover, the derivative displayed a Zn<sup>2+</sup>-induced red-shift of emission (44 nm), showing a color change from blue to light cyan under a 365-nm UV lamp. Its practical imaging applicability for intracellular Zn<sup>2+</sup> was confirmed in HeLa cells using a confocal microscope. The improved emission properties and cell imaging capability would provide a new approach to fluorescence sensation for Zn<sup>2+</sup>.

Keywords: Colorimetric sensor; ratiometric sensor; phenanthroline-imidazole; iron(II) ion; zinc ion

#### 1. Introduction

Metal ions play vital roles in biological and environmental processes. For instance, iron ion (Fe<sup>2+</sup>/Fe<sup>3+</sup>), the most abundant transition metal in cellular systems, exists widely in enzymes, proteins, and transcriptional events.<sup>1</sup> Compared to stable Fe<sup>3+</sup>, the presence of labile Fe<sup>2+</sup> holds particular significance due to its involvement in oxygen metabolism and intracellular electron transfer processes, which are crucial for various biological functions.<sup>2</sup> Either excess or deficiency of Fe<sup>2+</sup> can disturb cellular homeostasis and metabolism, leading to severe diseases,<sup>3-5</sup> such as anemia, cardiovascular diseases, and cancer. Zinc ion (Zn<sup>2+</sup>), the second most abundant metal in the human body, plays a crucial role in modulating brain excitability and is essential for various physiological processes, including immune system function, cell division, wound healing,

and synaptic plasticity.  $^{6-8}$  Moreover, the level abnormality of  $Zn^{2+}$  is associated with retarded growth in children, high blood cholesterol, and neurodegenerative disorders such as Alzheimer's and Parkinson's diseases.  $^{6,7}$  In natural environment, the accumulation of excess  $Zn^{2+}$  can reduce the soil microbial activity and result in phytotoxic effects. Therefore, the concentrations of metal ions must be regulated.

At present, a variety of techniques are available for quantitative analysis of metal ions, including atomic absorption/emission spectroscopy, polarography, voltammetry, flow injection, fluorescent probe, etc.<sup>2,3,9–11</sup> Among these detection methods, fluorescent sensors possess several advantages including simplicity, high sensitivity, rapid response to fluorogenic and colorimetric changes and cost-effectiveness. Optical cellular imaging with fluores-

cent probes has been an efficient approach for detecting metal ions in living cells. Therefore, highly selective and sensitive fluorescent sensors that use color and fluorescence intensity or shift are widely used in studies of biological analytes. 12-14 Ratiometric fluorescent probes have garnered increasing attention due to their exceptional properties, including signal read-out independent of instruments and environment, minimal auto-fluorescence, rapid response time, high spatial resolution, and remarkable contrast. 15-18 Additionally, compared to one-to-one chemosensors, using a single chemosensor for detecting multiple targets through differential responses, such as colorimetric or fluorescent spectral changes, offers enhanced efficiency and cost-effectiveness. 19-22 In this context, many of fluorescent probes for Zn<sup>2+</sup> have been developed.6-9,23 However, most of them suffer from the interference of Cd<sup>2+</sup> due to their similar properties as these two metal ions belong to the same group in the periodic table. 6,24,25 Moreover, achieving selective sensing of iron in both oxidation states (Fe<sup>2+</sup>/Fe<sup>3+</sup>) using a colorimetric probe that provides distinct signals easily visualized by the naked eye has posed a significant challenge. 10, 26 Therefore, there is an urgent need for the development of a highly selective, facile, simple, and efficient probe capable of detecting  $Fe^{2+}$  and  $Zn^{2+}$ .

The 1,10-phenanthroline (phen) framework serves as an excellent platform for the construction of chemosensors due to its favorable electro- and photoactive properties. 27-29 Nawaz et al. have previously reported a cellulose-based sensor incorporating phen, enabling selective detection of Fe2+ through both visual observation and fluorescent dual modes.<sup>30</sup> Additionally, a polyacrylamide-immobilized phen has been developed as a visual strip sensor to determine Fe<sup>2+</sup> ion precisely.<sup>31</sup> Moreover, phen derivatives can function as both fluorophores and ionophores for Zn<sup>2+</sup>, exhibiting discernible changes in fluorescence intensity and specific emission shift upon binding with Zn<sup>2+</sup> ion.<sup>32-34</sup> Considering these factors, we prepared a hybrid fluorescent sensor derived from the Debus-Radziszewski reaction, namely (2-(3,5-di(pyridin-4-yl)phenyl)-1-p-tolyl-1H-imidazo[4,5-f][1,10]phenanthroline) (1) (Scheme 1). The spectroscopic properties and potential application of the compound were systematically investigated. It was observed that compound 1 exhibited a rapid chromogenic response to Fe<sup>2+</sup> in the EtOH-HEPES buffer, transitioning from a colorless state to red. Additionally, compound 1 demonstrated highly selective and ratiometric fluorescence signals for  $\rm Zn^{2+}$  compared to other tested metal ions. The imaging capability of compound 1 for  $\rm Zn^{2+}$  was confirmed through microscopic imaging in living cells.

# 2. Experimental

#### 2. 1. Materials and Apparatus

All chemical reagents were commercially available and of analytical grade. The various metal ions were purchased from Aladdin (Shanghai, China), 1,10-phenanthroline-5,6-dione was purchased from TCI (China). The intermediate 3,5-di(pyridin-4-yl)benzaldehyde was synthesized according to the reported procedure. The NMR were measured by a Bruker DRX-400 spectrometer. IR spectra were taken on a Vector22 Bruker spectrophotometer (400–4000 cm<sup>-1</sup>) with KBr pellets. UV-vis absorption spectra were recorded on Hitachi U-3300 spectrophotometer. Fluorescence emission spectra were determined on Hitachi F-4500. The pH values of sample solutions were monitored by a PHS-3 system. Electrospray mass spectra (ESI-MS) were recorded on a Thermo Fisher LCQ-Fleet mass spectrometer.

# 2. 2. Synthetic Procedure

1,10-phenanthroline-5,6-dione (2.10 g, 10 mmol), 3,5-di(pyridin-4-yl)benzaldehyde (2.60 g, 10 mmol), p-toluidine (1.61 g, 15 mmol), NH<sub>4</sub>OAc (3.85 g, 50 mmol) were mixed in a 40 mL glacial acetic acid at room temperature. The mixture was heated at 120 °C for 20 h under stirring. After pouring the mixture into the water (30 mL), the red precipitation was filtered and purified by column chromatography using dichloromethane/methanol (20: 1, v/v) as eluent to afford 1 as gray-white powder with yield of 60%. IR (KBr, cm<sup>-1</sup>): 3379, 2980, 2923, 1590, 1560, 1551, 1518, 1492, 1452, 1433, 1400, 1379, 1318, 1294, 1223, 1155, 1217, 1087, 1017, 992, 890, 864, 833, 815, 791, 738, 721, 699, 689, 667, 643, 612, 539, 504, 485. ¹H NMR (400 MHz, CDCl<sub>3</sub>)  $\delta$ : 2.63 (s, 3H), 7.32 (dd, J = 4.0, 8.4 Hz, 1H), 7.37 (d, J = 6.0 Hz, 4H), 7.51–7.61 (m, 5H), 7.72–7.75 (dd, J =

$$\begin{array}{c} O & O \\ O & O \\ N & N \end{array} \begin{array}{c} O & O \\ N & N \end{array}$$

Scheme 1. Synthesis of 1.

4.4, 8.0 Hz, 1H), 7.81 (s, 1H), 7.92 (d, J = 1.6 Hz, 2H), 8.68 (d, J = 6.0 Hz, 4H), 9.05 (dd, J = 1.6, 4.4 Hz, 1H), 9.13 (dd, J = 1.6, 8.0 Hz, 1H), 9.18 (dd, J = 1.6, 4.4 Hz, 1H). ESI-MS: 541.4200 (M<sup>+</sup>). Anal. Calcd for  $C_{36}H_{24}N_6$ : C, 79.98; H, 4.47, N, 15.55. Found: C, 79.75; H, 4.46, N, 15.61%.

# 2. 3 Single-Crystal X-Ray Diffraction

Colorless single crystals of 1 were obtained by evaporation of its methanol solution at room temperature. Crystal diffraction data were collected on a Bruker SMART APEX CCD-based diffractometer (Cu-K $\alpha$  radiation,  $\lambda$  = 1.54184 Å). Multi-scan absorption corrections were applied by SADABS.<sup>36</sup> The structure was solved by direct methods and refined on  $F^2$  by full-matrix least-squares with the Bruker's SHELXS program.<sup>37</sup> All the non-hydrogen atoms were located in the Fourier maps and refined with anisotropic parameters. Hydrogen atoms were placed in their geometrically idealized positions and constrained to ride on their parent atoms. Crystallographic data in CIF format has been deposited in the Cambridge Crystallographic Data Centre (CCDC) under deposition number 2042300. Details of crystallographic data are summarized in Table S1.

# 2. 4. General Methods for Spectroscopic Analysis

The stock solutions (6 mM) of metal ions (Mn(NO<sub>3</sub>)<sub>2</sub> · 4H<sub>2</sub>O, Pb(NO<sub>3</sub>)<sub>2</sub>, Co(NO<sub>3</sub>)<sub>2</sub> · 6H<sub>2</sub>O, Zn(NO<sub>3</sub>)<sub>2</sub> · 6H<sub>2</sub>O, Cu(NO<sub>3</sub>)<sub>2</sub> · 3H<sub>2</sub>O, Ni(NO<sub>3</sub>)<sub>2</sub> · 6H<sub>2</sub>O, Cd(NO<sub>3</sub>)<sub>2</sub> · 4H<sub>2</sub>O, HgCl<sub>2</sub>, FeSO<sub>4</sub> · 7H<sub>2</sub>O, Fe<sub>2</sub>(SO<sub>4</sub>)<sub>3</sub>, CaCl<sub>2</sub> · 2H<sub>2</sub>O, MgCl<sub>2</sub>, NaCl, and KCl) were prepared in doubly distilled water. **1** was dissolved in spectroscopic pure ethanol to give the stock solution (5 mM). The measurements of both UV-vis absorption and fluorescence spectra were conducted in the solution of HEPES buffer with pH 7.2 containing 50% ethanol (v/v 50  $\mu$ M) at room temperature. For the metal ions titration, aliquots of 25  $\mu$ L aqueous metal cation solution were added to the 3 mL diluted **1** solution. The measurements were carried out in 1 min after the addition.

#### 2. 5. Cell Culture and Fluorescence Imaging

HeLa cells were cultured in Dulbecco's Modified Eagle Medium, which was supplemented with 10% fetal bovine serum, penicillin (100 units/mL), streptomycin (100 mg/mL) and 5% CO $_2$  at 37 °C. After removing the incubation media and rinse with PBS for three times, the cells were treated with 1 (10  $\mu M$ ) for additional 60 min at room temperature. Then the cells were washed three times with PBS before observation. The fluorescence images were captured on Zeiss LSM 710 microscope equipped with a 63×oil-immersion objective. For the imaging of HeLa cells with exogenous Zn $^{2+}$ , the exogenous Zn $^{2+}$  was introduced by incubating the cells with 5 $\mu M$  ZnSO $_4$ / pyrithione solu-

tion. After imaging, the cells of exogenous  $Zn^{2+}$  were further treated with  $50\,\mu M$  TPEN (N, N, N, N-tetrakis(2-pyridylmethyl)ethylenediamine) solution (prepared by diluting the TPEN stock solution with PBS) to scavenge the intracellular  $Zn^{2+}$ . Then the cells were rinsed with PBS and imaged. For all imaging, the samples were excited at 405 nm, and the band pass is 440-520 nm.

## 3. Results and Discussion

#### 3. 1. Synthesis and Characterization

The probe was constructed by conjugating 3,5-di(pyridin-4-yl)benzene into a fused imidazole/phen system *via* a one-step Debus-Radziszewski reaction. The enlarged conjugated system in 1 and the chelating effect of phenanthroline are expected to report the presence of specific metal cation by triggering the emission change.

The structure of 1 was characterized using FT-IR, <sup>1</sup>H NMR, and ESI-MS techniques (Figures. S1-S3). The molecular structure of 1 was also confirmed by single-crystal X-ray diffraction analysis. The crystal structure of 1 with the atom numbering scheme is shown in Figure 1.

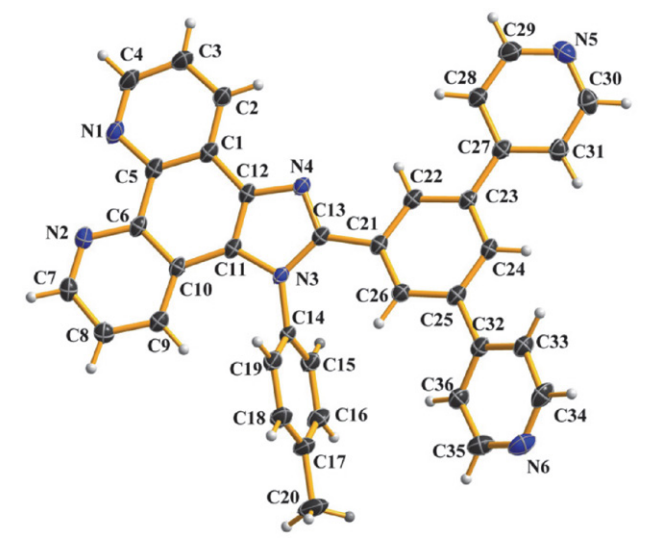


Figure 1. Crystal structure of 1.

1 was crystallized in the triclinic system with the space group  $P\bar{1}$ . Each unit cell contains two molecules (Z=2). 1 features a non-planar structure. The dihedral angle between the para-toluene ring and the imidazole ring is  $80.03(1)^\circ$ ; the dihedral angle between the two pyridine rings is  $37.52(1)^\circ$ . The C14-N3 bond length (1.44 Å) is shorter than the standard C-N single bond length (1.47 Å), which may be attributed to the existence of ICT transition between the para-toluene ring and the phen subunit.  $^{38,39}$ 

The intramolecular hydrogen bond is formed *via* C22-H22···N4; meanwhile, the molecules of **1** are connect-

ed by C30-H30···N1<sup>i</sup> (symmetry code: (i) 1+x, 1+y, z) (Figure S4). As shown in Figure S5, the free methanol molecules are located between these 1D supramolecular chains and serve as hydrogen bonding acceptors and donors, linking these chains into a 2D sheet structure extended in crystallographic *ac* plane. *via* C4-H4···O1<sup>ii</sup>, C35-H35···O1<sup>ii</sup>, O1-H1···N5<sup>iv</sup> (symmetry code: (ii) -1+x, y, 1+z; (iii) x, 1+y, z; (iv) x, -1+y, -1+z).

that it was visual by a solution color change from blue to light cyan under a UV lamp only when  $\mathrm{Zn^{2+}}$  was added into the 1 solution (Figure 2b). The visual detection observation indicated the selectivity towards  $\mathrm{Fe^{2+}}$  and  $\mathrm{Zn^{2+}}$  ions, prompting us to conduct further investigations on the metal ion recognition capability using different spectral techniques.

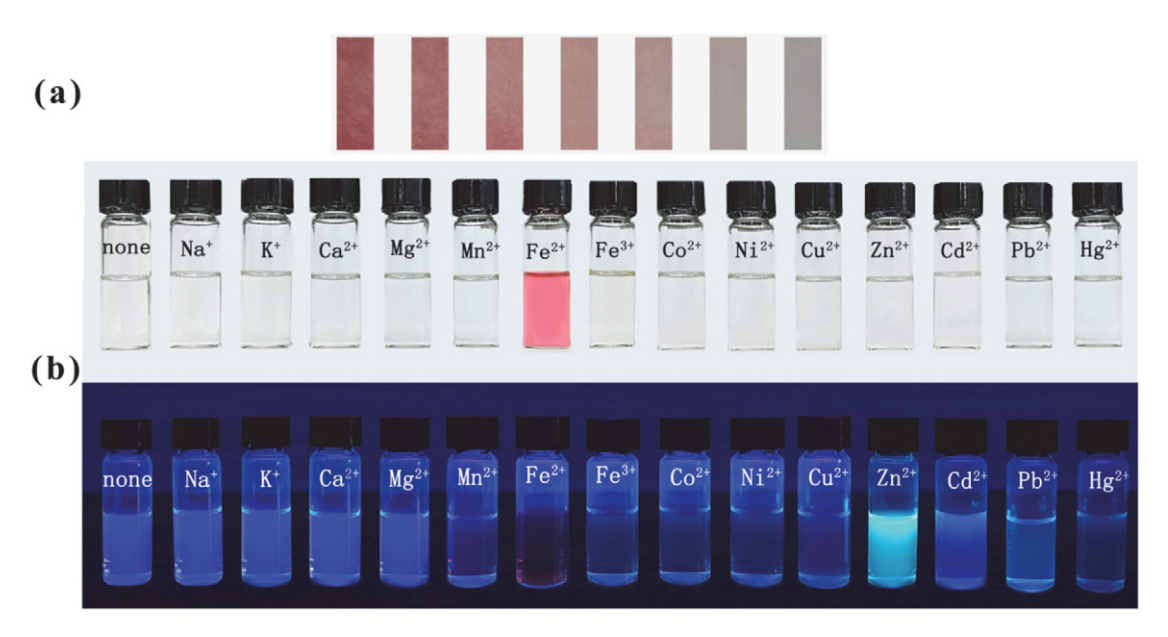


**Figure 2.** (a) Photograph of **1** test strips wetted by solutions containing  $1.0 \times 10^{-2}$ ,  $5.0 \times 10^{-3}$ ,  $1.0 \times 10^{-3}$ ,  $5.0 \times 10^{-4}$ ,  $1.0 \times 10^{-4}$ ,  $1.0 \times 10^{-5}$ , 0 M of FeCl<sub>2</sub> (from left to right). (b) Photograph of **1** (50  $\mu$ M) in EtOH-HEPES buffer (1:1, v:v, pH 7.2) solutions containing different metal cations (1 equiv) under visible light (upper row) and UV lamp (lower row).

## 3. 2. Visual Detection

The selectivity of a fluorescent sensor is a crucial factor for evaluating its performance. The selectivity of a fluorescent sensor is a crucial factor for evaluating its performance. The visual method was employed to investigate the metal ion recognition capability of compound 1. 1 was treated with 14 kinds of different metal ions (Na+, K+, Ca<sup>2+</sup>, Mg<sup>2+</sup>, Mn<sup>2+</sup>, Fe<sup>2+</sup>, Fe<sup>3+</sup>, Co<sup>2+</sup>, Ni<sup>2+</sup>, Cu<sup>2+</sup>, Zn<sup>2+</sup>, Cd<sup>2+</sup>, Pb<sup>2+</sup> and Hg<sup>2+</sup>) to study its sensitivity and selectivity towards particular metal ions. Upon adding an equivalent amount of respective metal ion into compound 1, only the presence of Fe<sup>2+</sup> resulted in an instantaneous colorimetric response from colorless to pink under visible light (Figure 2a), which can be easily distinguished by naked-eye. However, no change in color was observed when other cations, including excess amounts of Fe3+ ions (5 equiv), were added. Probe 1 was coated on nitrocellulose papers to obtain the test papers. Figure 2a confirms the visual color change phenomena of indicator paper with different concentrations of  $Fe^{2+}$ . Consequently, when coating substrate 1, the resulting materials can be utilized as a qualitative analysis tool for metal ions, serving as a test paper. We also noted

# 3. 3. Investigations Using UV-VIS Spectrophotometry

The colorimetric sensing performance of sensor 1 was investigated through UV-vis titration with various transition metal cations. A 50 µM solution of the sensor was utilized in the presence of 1 equiv of different metal ions for each experiment. The resulting UV-vis titration spectra are presented in Figure 3. In the HEPES buffer solution, sensor 1 exhibited strong absorption bands below 400 nm, corresponding to the  $\pi$ - $\pi$ \* transitions (245) nm,  $\epsilon = 5.9 \times 10^4 \text{ L mol}^{-1} \text{ cm}^{-1}$ ; 270 nm,  $\epsilon = 6.3 \times 10^4 \text{ L}$  $\text{mol}^{-1} \text{ cm}^{-1}$ ; 320 nm,  $\varepsilon = 2.1 \times 10^4 \text{ L mol}^{-1} \text{ cm}^{-1}$ ) (Figure 3a). With the addition of Fe<sup>2+</sup> into 1, a new band centered at 528 nm appeared in the spectra (Figure 3a) and increased linearly with the [Fe<sup>2+</sup>]<sub>total</sub> (Figure 3b). The absorption enhancement reached saturation when the quantity of Fe<sup>2+</sup> reached 0.5 equiv of sensor 1, implicating a complexation ratio 2:1 between 1 and Fe2+ (Figures. 3b and 3c). Further increments in [Fe<sup>2+</sup>] did not yield any additional enhancements. Other metal ions did not cause any significant changes at 528 nm under identical conditions (Figure 3a). The distinct color change might be as-

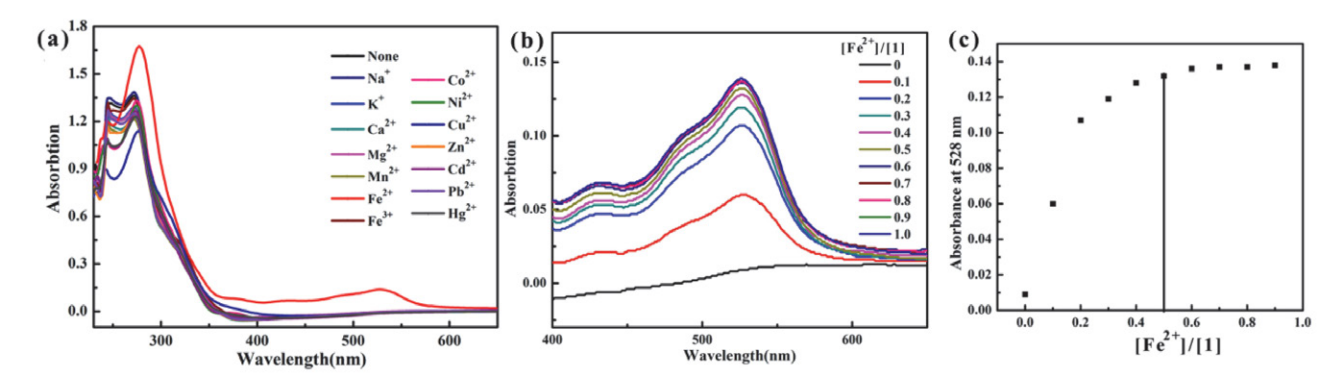


Figure 3. (a) UV-vis titration of 1 (50  $\mu$ M) with different transition metal cations (1.0 equiv) in EtOH-HEPES buffer (1:1, v:v, pH 7.2) media. (b) UV-vis spectra of 1 (50  $\mu$ M) upon Fe<sup>2+</sup> (6 mM) titration in EtOH-HEPES buffer (1:1, v:v, pH 7.2) media. (c) The titration profile of the absorbance at 528 nm.

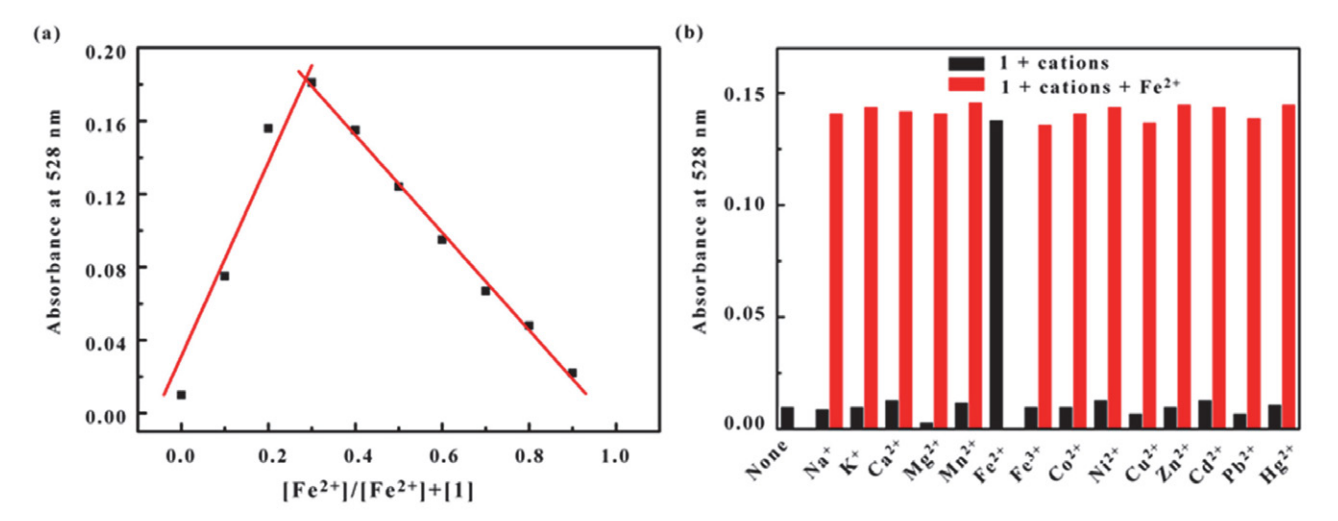


Figure 4. (a) Job's plot for the interaction of 1 with Fe<sup>2+</sup> ions in EtOH-HEPES buffer (pH = 7.2). The total molar concentration of 1 and Zn<sup>2+</sup> is 50  $\mu$ M. (b) Absorbance at 528 nm of 1 (50  $\mu$ M). Black bars represent the absorbance of free sensor or in the presence of different metal cations. Red bars, the absorbance determined after the addition of 1.0 equiv of competitive metal ions followed by the addition of 1.0 equiv of Fe<sup>2+</sup>.

cribed to the metal-to-ligand charge-transfer (MLCT) band at 528 nm due to the Fe<sup>2+</sup> coordination to the phenanthroline moiety.

To better understand the stoichiometry of  $1\text{-Fe}^{2+}$  complex, Job's plot analysis was performed. The total sum of the concentration of 1 and the Fe<sup>2+</sup> was kept constant, and the Fe<sup>2+</sup> mole fraction was varied between 0.0 and 0.9. As shown in Figure 4a, the appearance of maximum  $A_{528}$  around the 0.3 molar fractions indicates that the stoichiometry of the complex formed between 1 and Fe<sup>2+</sup> would be 2:1. The proposed coordination mechanism is shown in Scheme S1.

Competitive experiments were also carried out by adding 1.0 equiv of Fe<sup>2+</sup> to solutions containing 5.0 equiv of other chosen metal ions in EtOH-HEPES buffer (1:1, v:v, pH 7.2). The results shown in Figure 4b indicated that the competitive metal ions had no substantial interference with detecting Fe<sup>2+</sup>. Therefore, it is clear that 1 can detect Fe<sup>2+</sup> selectively. The colorimetric limitation of detection (LOD) for Fe<sup>2+</sup> is determined as  $1.0 \times 10^{-6}$  M ( $3\sigma/\text{slope}$ ).<sup>24</sup>

As stated above, the UV-vis titration spectra characteristics are consistent with the results of visual detection.

#### 3. 4. Fluorescence Spectral Study

To gain insight into the fluorescent sensing capability of 1 towards metal ions, fluorometric titration was conducted in EtOH-HEPES buffer (1:1, v:v, pH 7.2) at room temperature. Free 1 exhibited an emission band centered at 412 nm upon exciting at 350 nm. As shown in Figure 5a, cations such as Na<sup>+</sup>, K<sup>+</sup>, Ca<sup>2+</sup> and Mg<sup>2+</sup> lead to an almost silent fluorescent response, while Fe<sup>3+</sup>, Cu<sup>2+</sup>, Mn<sup>2+</sup> and Co<sup>2+</sup> triggered emission quenching. Different degrees of fluorescent intensity reduction were observed when Cd<sup>2+</sup>, Fe<sup>2+</sup>, Pb<sup>2+</sup>, Ni<sup>2+</sup> and Hg<sup>2+</sup> were added to the system containing sensor 1. Additionally, the addition of Zn<sup>2+</sup> resulted in a distinct red-shifted emission from 412 to 456 nm. These observations substantiated the results of the visual detection experiment (Figure 2b) that 1 is highly selective

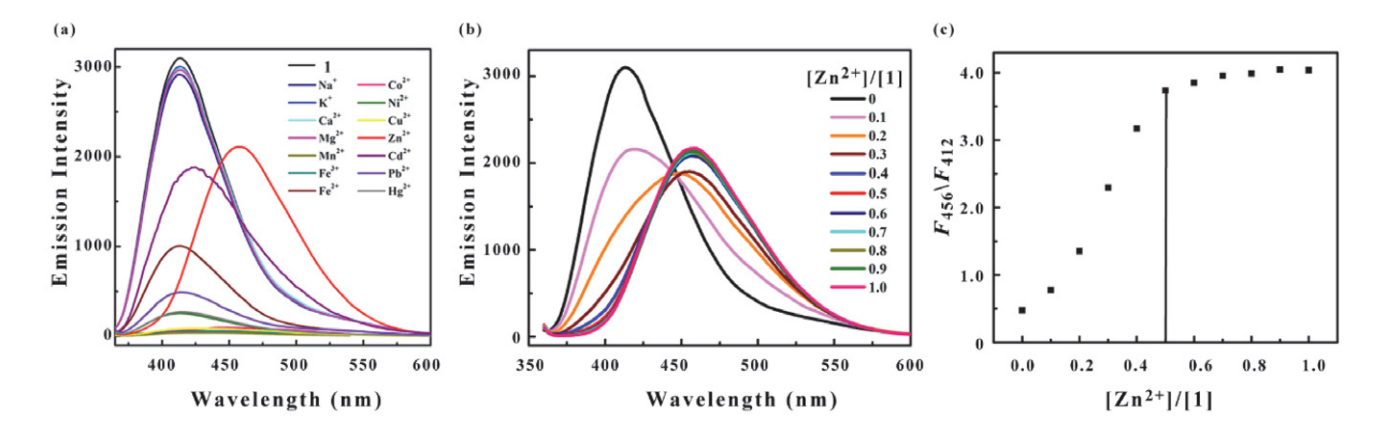


Figure 5. (a) Emission spectra of 1 (50  $\mu$ M) in presence of various metal ions (1.0 equiv) in EtOH-HEPES buffer (v/v, 1/1, pH 7.2) (b) Emission spectra of 1 (50  $\mu$ M) obtained upon Zn<sup>2+</sup> (6 mM) titration. (c) The titration profile based on the emission ratio at 456 and 412 nm,  $F_{456}/F_{412}$ .

towards  $Zn^{2+}$ . The fluorescence bathochromic shift can be attributed to the intraligand transitions ( $\pi$ – $\pi$ \* transitions).

The dose-dependent fluorescence responses of 1 to Zn<sup>2+</sup> were also measured. The fluorescence intensity decreased by 30% when 0.1 equiv Zn2+ was added into solution 1. Meanwhile, the maximum peak of the fluorescence red-shifted with an increase of Zn2+ dosage. Upon gradually adding of 0.3 equiv Zn<sup>2+</sup>, the fluorescence emission peak shifted to 456 nm. The fluorescence intensity at 456 nm continued to increase until 0.5 equiv Zn<sup>2+</sup> was added. The ratio of the emission intensity at 456 and 412 nm ( $F_{456}$ /  $F_{412}$ ) also showed a linear enhancement with the increasing  $[Zn^{2+}]_{total}$  until the ratio of  $[Zn^{2+}]_{total}/[1]$  reached 1:2 (Figures. 5b, 5c). After that, the emission spectra of 1 became stable. The remarkable bathochromic shift made 1 a potential ratiometric sensor for Zn<sup>2+</sup>. In particular, 1 can distinguish Zn<sup>2+</sup> from the chemically similar Cd<sup>2+</sup>, whereas the discrimination of  $Zn^{2+}$  from  $Cd^{2+}$  is well known to be a major obstacle in many cases. 24,25 The atomic radius of  $Cd^{2+}(0.97 \text{ Å})$  is much larger than that of  $Zn^{2+}(0.74 \text{ Å})$ , and probably does not fit well into the chelate cavity of phenanthroline. The fluorimetric LOD of **1** for  $Zn^{2+}$  is  $7.1 \times 10^{-7}$  M.

The stoichiometry between 1 and  $Zn^{2+}$  was also determined using Job's continuous variation method. Results demonstrate that the fluorescence intensity  $F_{456}/F_{412}$  ratio of the solution reaches the maximum at a mole fraction of approximately 0.34 for  $Zn^{2+}$  (Figure 6a), indicating a 2:1 complexation stoichiometry between 1 and  $Zn^{2+}$ . The proposed coordination mechanism is also depicted in Scheme S1

To investigate the applicability of 1 as a  $\rm Zn^{2+}$  selective fluorescence sensor, competition experiments were carried out by mixing  $\rm Zn^{2+}$  with various common metal ions. The results shown in Figure 6b indicated that no significant alteration in the fluorescence intensity ratio  $F_{456}/F_{412}$  was observed in the presence of other selected metal ions. Furthermore, the presence of Na<sup>+</sup>, K<sup>+</sup>, Ca<sup>2+</sup>, and Mg<sup>2+</sup>, abundant in cells, did not interfere with the ratiom-

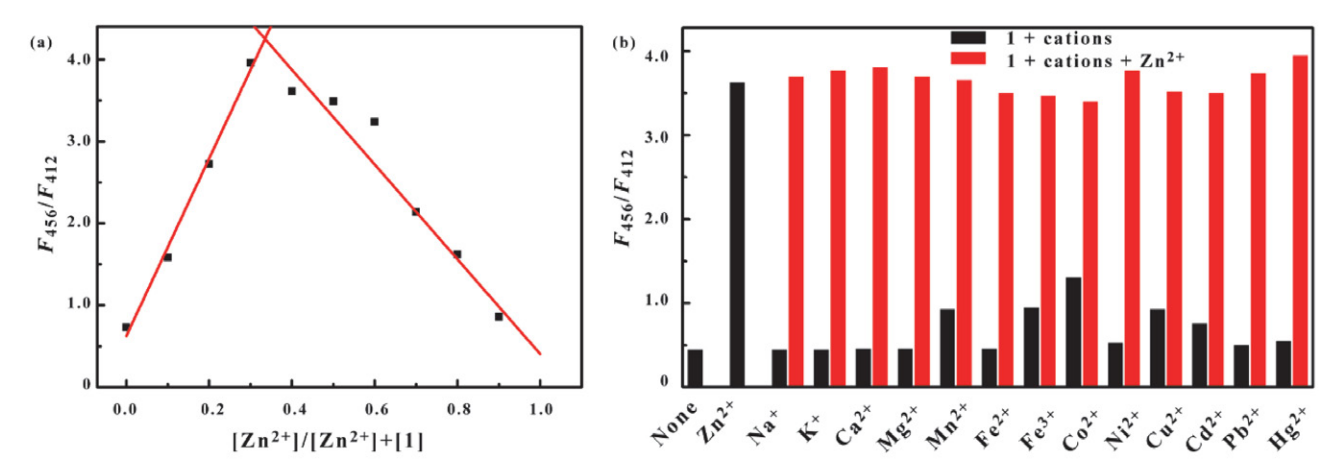


**Figure 6.** (a) Job's plot of Zn-1 complex in EtOH-HEPES buffer (1:1, v:v, pH 7.2). The total molar concentration of 1 and Zn<sup>2+</sup> is 50 μM. (b) Emission ratio at 456 and 412 nm ( $F_{456}/F_{412}$ ) of 1 (50 μM) in EtOH-HEPES buffer (1:1, v:v, pH 7.2). Black bars represent the  $F_{456}/F_{412}$  ratio of the free sensor or in the presence of different metal cations. Red bars represent the  $F_{456}/F_{412}$  ratio of 1 determined after the addition of indicated metal ions followed by the addition of 1 equiv of Zn<sup>2+</sup>. The final concentration is 50 μM for Zn<sup>2+</sup>, Mn<sup>2+</sup>, Fe<sup>2+</sup>, Fe<sup>3+</sup>, Co<sup>2+</sup>, Ni<sup>2+</sup>, Cu<sup>2+</sup>, Cd<sup>2+</sup>, Pb<sup>2+</sup> and Hg<sup>2+</sup>, for Na<sup>+</sup>, K<sup>+</sup>, Ca<sup>2+</sup> and Mg<sup>2+</sup> is 50 mM.

etric response to  $Zn^{2+}$ , even though their concentration was 1000 times higher than  $[Zn^{2+}]$ . These results indicated that the recognition of  $Zn^{2+}$  by 1 remained unaffected by the coexistence of other metal ions.

The pH value of environment may affect the performance of sensor in the practical application. The pH dependency of **1** toward the detection of  $Zn^{2+}$  was investigated (Figure S6). Fluorescent pH titration of **1** and **1**+ $Zn^{2+}$  complex showed a relatively stable  $F_{456}/F_{412}$  ratio from pH 4.0–8.0, making it suitable for physiological detection applications.

# 3. 5. Cell Imaging

 $Zn^{2+}$  is a crucial metal ion the human body requires in various fundamental biological processes. Therefore, the practical application of  ${\bf 1}$  in the biological system was further checked with HeLa cells for fluorescence imaging studies. In order to reduce irradiation damage, a 405 nm laser was selected as the excitation source. Because the emission wavelength of  ${\bf 1}$  (412 nm) is close to 405 nm, only the single green channel (band path 440–520 nm) was employed. The imaging experiment selected TPEN as the fluorescence quenching reagent toward  ${\bf 1}$ -Zn<sup>2+</sup>. Before imaging, the cells were incubated with  ${\bf 1}$  (10  $\mu$ M) for 60 min.

cell. According to the relative fluorescence intensity analyzed by Image Pro-Plus 6.0, the average fluorescence intensity of cells before introducing exogenous  $Zn^{2+}$  is 8.25, while that for cells with exogenous  $Zn^{2+}$  is 17.15. The result suggests that 1 can bind to intracellular  $Zn^{2+}$ , enhancing fluorescence emission. When 50  $\mu M$  TPEN was introduced into media, a more stable complex was formed between TPEN and  $Zn^{2+}$  generating the fluorescence reduction. The average fluorescence intensity of cells recovered to 8.13. Cell imaging experiment results indicate that 1 can be used for fluorescence imaging of  $Zn^{2+}$  in living cells.

#### 4. Conclusion

In summary, we successfully synthesized and characterized phenanthroline-modified chemosensor 1. Our results demonstrate that sensor 1 exhibits remarkable colorimetric sensing ability towards  $Fe^{2+}$  ions. Moreover, it is an excellent sensitive and selective ratiometric fluorescence probe for  $Zn^{2+}$  in buffer-ethanol solutions. The coordination mode between 1 and  $Fe^{2+}$  or  $Zn^{2+}$  was confirmed to be 2:1 based on titration profile analysis and Job's plot analysis. Notably, the proposed sensor displays high sensitivity, selectivity for dual-sensing of  $Fe^{2+}$  or  $Zn^{2+}$ , pH-in-

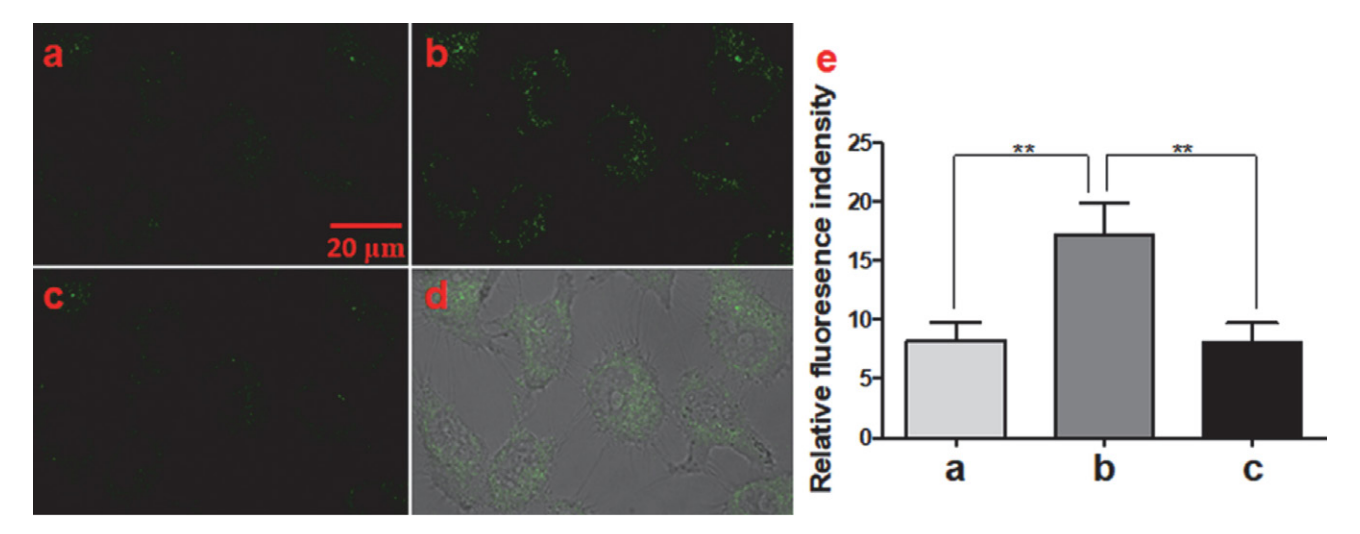


Figure 7. Confocal fluorescence imaging of intracellular  $Zn^{2+}$  in HeLa cells stained by 1 solution (10  $\mu$ M in PBS) at 25 °C for 60 min. (a) HeLa cells preincubated in 10  $\mu$ M 1 solution at room temperature (25 min). (b) Rinsed HeLa cells (1 × PBS, three times) in (a) were further incubated in 5  $\mu$ M  $ZnSO_4/$  pyrithione (1:1) solution, followed by rinsing with 10  $\mu$ M 1 solution. (c) HeLa cells in (b) rinsed with 50  $\mu$ M TPEN solution. (d) overlay between (a) and bright field. (e) Relative fluorescence intensities of (a), (b) and (c) analyzed with Image Pro-Plus 6.0. \*\* P < 0.05, significantly different compared with (b).

The results of fluorescence imaging were presented in Figure 7. After incubation with 1 solution (10  $\mu$ M in PBS, DMSO/water = 1:99, v/v) at 25 °C for 60 min, the bright fluorescence inside the cells indicated that 1 can be loaded into cells, suggesting the membrane permeability of 1. When exogenous Zn<sup>2+</sup> was introduced *via* incubation with 5 $\mu$ M ZnSO<sub>4</sub>/ pyrithione solution, an image of obvious fluorescence enhancement was observed inside the

dependent emission behavior, and cell imaging capability. These findings highlight the potential of our developed sensor in facilitating the advancement of more efficient and practical methods for detecting Fe<sup>2+</sup> or Zn<sup>2+</sup> ions. Due to its limited water solubility, the current probe cannot be directly utilized in biological environments. As part of our ongoing research, we are investigating the feasibility of incorporating the probe onto water-soluble nanomaterials.

#### **Supplementary Material**

Crystallographic data (excluding structure factors) for the structural analysis have been deposited with the Cambridge Crystallographic Data Center as supplementary publication Nos. CCDC 2042300 (1). Copies of the data can be obtained free of charge via www.ccdc.ac.uk/conts/retrieving.html (or from The Director, CCDC, 12 Union Road, Cambridge CB2 1EZ, UK, Fax: +44-1223-336-033. E-mail: deposit@ccdc.cam.ac.uk).

#### Acknowledgement

We are grateful for financial support from National Natural Science Foundation of China (Nos. 21771120 and 82104112).

## 5. References

- P. Li, L. B. Fang, H. Zhou, W. Zhang, X. Wang, N. Li, H. B. Zhong, B. Tang, *Chem.-Eur. J.* 2011, *17*, 10520–10523.
   DOI:10.1002/chem.201101327
- 2. A. Parsaei-Khomami, A. Badiei, Z. S. Ghavami, J. B. Ghasemi, *J. Mol. Struct.* **2022**, *1252*, 131978–131988.

DOI:10.1016/j.molstruc.2021.131978

- S. Santhoshkumar, K. Velmurugan, J. Prabhu, G. Radhakrishnan, R. Nandhakumar, *Inorg. Chim. Acta* 2016, 439, 1–7. DOI:10.1016/j.ica.2015.09.030
- 4. S. Kamali, M. Orojloo, S. Amani, *J. Mol. Struct.* **2021**, *1243*, 130708–130716. **DOI:**10.1016/j.molstruc.2021.130708
- A. Finelli, V. Chabert, N. Hérault, A. Crochet, C. Kim, K. M. Fromm, *Inorg. Chem.* 2019, 58, 13796–13806.
   DOI:10.1021/acs.inorgchem.9b01478
- H. H. Song, Z. Zhang, *Dyes Pigment*. 2019, 165, 172–181.
   DOI:10.1016/j.dyepig.2019.02.011
- Y. X. Sun, W. M. Ding, J. Li, Y. H. Jia, G. Guo, Z. P. Deng, J. Mol. Struct. 2022, 1252, 132219–132229.
   DOI:10.1016/j.molstruc.2021.132219
- 8. J. Y. Koh, S. W. Suh, B. J. Gwag, Y. Y. He, C. Y. Hsu, D. W. Choi, *Science* **1996**, *272*, 1013–1016.

DOI:10.1126/science.272.5264.1013

- X. J. He, F. Ding, X. S. Sun, Y. J. Zheng, W. Xu, L. S. Ye, H. Chen, J. L. Shen, *Inorg. Chem.* 2021, 60, 5563–5572.
   DOI:10.1021/acs.inorgchem.0c03456
- X. P. Yang, Y. S. Wang, R. Liu, Y. R. Zhang, J. Tang, E. B. Yang,
   D. Zhang, Y. F. Zhao, Y. Ye, Sens. Actuator B-Chem. 2019, 288,
   217–224. DOI:10.1016/j.snb.2019.02.123
- 11. N. Dey, ACS Appl. Bio Mater. **2021**, *4*, 6893–6902. **DOI:**10.1021/acsabm.1c00600
- N. Tomer, A. Goel, P. Bhalla, P. Bhagat, R. Malhotra, *J. Photochem. Photobiol. A-Chem.* 2022, 427, 113823–113838.
   DOI:10.1016/j.jphotochem.2022.113823
- A. K. Manna, J. Monda, K. Rout, G. K. Patra, Sens. Actuator B-Chem. 2018, 275, 350–358.
   DOI:10.1016/j.snb.2018.08.060
- 14. K. Naik, V. Revankar, J. Fluoresc. 2018, 28, 1105-1114.

- **DOI:**10.1007/s10895-018-2273-9
- Y. Liu, L. Bai, Y. H. Li, Y. Ni, C. Q. Xin, C. W. Zhang, J. H. Liu,
   Z. P. Liu, L. Li, W. Huang, Sens. Actuator B-Chem. 2019, 279,
   38–43. DOI:10.1016/j.snb.2018.09.107
- G. R. C. Hamilton, S. Kaur, S. Kamila, B. Callan, J. F. Callan, New J. Chem. 2018, 42, 14986–14993.
   DOI:10.1039/C7NJ04520D
- A. Mukherjee, P. C. Saha, R. S. Das, T. Bera, S. Guha, ACS Sens. 2021, 6, 2141–2146. DOI:10.1021/acssensors.1c00961
- R. Azadbakht, M. Koolivand, J. Khanabadi, *Anal. Methods* 2017, 9, 4688–4694. DOI:10.1039/C7AY01568B
- 19. S. M. Hwang, M. S. Kim, M. Lee, M. H. Lim, C. Kim, *New J. Chem.* **2017**, *41*, 15590–15600. **DOI:**10.1039/C7NJ03575F
- A. Mohammadi, J. Jabbari, Can. J. Chem. 2016, 94, 631–636.
   DOI:10.1139/cjc-2016-0039
- Y. S. Xie, J. Zhang, L. Yang, Q. X. Chen, Q. Hao, L. Zhang, H. Y. Sun, Front. Chem. Sci. Eng. 2022, 16, 121–127.
   DOI:10.1007/s11705-021-2051-0
- D. Singh, D. Rajput, S. Kanvah, Chem. Commun. 2022, 58, 2413–2429. DOI:10.1039/D1CC06944F
- M. V. Karmegam, S. Karuppannan, D. B. C. Leslee, S. Subramanian, S. Gandhi, *Luminescence* 2020, 35, 90–97.
   DOI:10.1002/bio.3701
- 24. H. He, Z. Cheng, L. Zheng, *J. Mol. Struct.* **2021**, *1227*, 129522–129529. **DOI**:10.1016/j.molstruc.2020.129522
- S. Mandal, Y. Sikdar, D. K. Malti, R. Sanyal, D. Das, A. Mukherjee, S. K. Mandal, J. K. Biswas, A. Bauzá, A. Frontera, S. Goswami, J. Photochem. Photobiol. A-Chem. 2017, 334, 86–100. DOI:10.1016/j.jphotochem.2016.10.038
- S. M. Feng, J. R. Zheng, J. Z. Zhang, Z. S. Gui, G. Q. Feng, Sens. Actuator B-Chem. 2022, 371, 132512–132520. DOI:10.1016/j.snb.2022.132512
- 27. X. Y. Ma, S. Y. Chen, H. Yu, Y. W. Guan, J. J. Li, X. W. Yan, Z. H. Zhang, *Nanoscale Res. Lett.* 2019, 14, 318–327.
  DOI:10.1186/s11671-019-3149-x
- K. Nehra, A. Dalal, A. Hooda, R. K. Saini, D. Singh, S. Kumar, *Polyhedron* **2022**, *217*, 115730–115736.
   **DOI:**10.1016/j.poly.2022.115730
- P. Alreja, N. Kaur, RSC Adv. 2016, 6, 23169–23217.
   DOI:10.1039/C6RA00150E
- H. Nawaz, W. G. Tian, J. M. Zhang, R. N. Jia, Z. Y. Chen, J. Zhang, ACS Appl. Mater. Interfaces 2018, 10, 2114–2121.
   DOI:10.1021/acsami.7b17342
- S. A. Kumar, N. Thakur, H. J. Parab, S. P. Pandey, R. N. Shinde,
   A. K. Pandey, S. D. Kumar, A. V. R. Reddy, *Anal. Chim. Acta* 2014, 851, 87–94. DOI:10.1016/j.aca.2014.08.047
- 32. R. Satheeshkumar, R. Rajamanikandan, M. Ilanchelian, K. Sayin, K. J. R. Prasad, *Spectroc. Acta Pt. A-Molec. Biomolec. Spectr.* 2019, 221, 21117196–21117206.
  - DOI:10.1016/j.saa.2019.117196
- B. Zhang, K. S. Cao, Z. A. Xu, Z. Q. Yang, H. W. Chen, W. Huang, G. Yin, X. Z. You, Eur. J. Inorg. Chem. 2012, 3844–3851. DOI:10.1002/ejic.201200423
- S. Karakaya, F. Algi, *Tetrahedron Lett.* **2014**, *55*, 5555–5559.
   **DOI:**10.1016/j.tetlet.2014.08.059
- 35. Y. Yu, X. M. Zhang, J. P. Ma, Q. K. Liu, P. Wang, Y. B. Dong,

*Chem. Commun.* **2014**, *50*, 1444–1446. **DOI:**10.1039/C3CC47723A

- S. G. M., SADABS, University of Gottingen 1996, Germany.
   G. M. Sheldrick, Acta Crystallogr. Sect. A 2008, 64, 112–122.
   DOI:10.1107/S0108767307043930
- C. Parthiban, K. P. Elango, Spectroc. Acta Pt. A-Molec. Biomolec. Spectr. 2017, 174, 147–153.
   DOI:10.1016/j.saa.2016.11.022
- K. Karaoglu, K. Kaya, I. Yilmaz, Dyes Pigment. 2020, 180, 108445–108454. DOI:10.1016/j.dyepig.2020.108445

# **Povzetek**

Sintetizirali smo nov derivat fenantrolina z imidazolno skupino, (2-(3,5-di(piridin-4-il)fenil)-1-p-tolil-1H-imidazo[4,5-f][1,10] fenantrolin). Spojina deluje kot multifunkcionalni senzor z visoko občutljivo kolorimetrično reakcijo na Fe $^{2+}$  ione in selektivno fluorescenčno reakcijo na Zn $^{2+}$  v raztopini pufer-etanol. Intenzivna barvna sprememba iz brezbarvne v rdečo ob dodatku Fe $^{2+}$  omogoča zaznavanje že s prostim očesom. Ob dodatku Zn $^{2+}$  opazimo premik emisije (44 nm) proti večjim valovnim dolžinam, kar pod obsevanjem z UV svetlobo valovne dolžina 365 nm povzroči spremembo barve iz modre v modrozeleno. Praktično uporabo za vizualizacijo intracelularnega Zn $^{2+}$  smo preizkusili na HeLa celicah s konfokalnim mikroskopom. Izboljšane emisijske lastnosti in sposobnost opazovanja celic omogočajo nov pristop k fluorescenčnemu zaznavanju Zn $^{2+}$ .



Except when otherwise noted, articles in this journal are published under the terms and conditions of the Creative Commons Attribution 4.0 International License